Am J Transl Res 2023;15(4):2656-2675
www.ajtr.org /ISSN:1943-8141/AJTR0145718

*Original Article*

# CD31 promotes diffuse large B-cell lymphoma metastasis by upregulating OPN through the AKT pathway and inhibiting CD8+ T cells through the mTOR pathway

Zhengchang He[1,2,3], Shaoxian Shen[4], Yuyao Yi[5], Lingli Ren[6], Huan Tao[7], Fujue Wang[8], Yongqian Jia[1,2,3,7]

*[1]Sichuan University, Chengdu 610000, Sichuan, PR China; [2]West China School of Medicine, Sichuan University, Chengdu 610000, Sichuan, PR China; [3]Hematological Institute of Sichuan Province, Chengdu 610000, Sichuan, PR China; [4]Sichuan Provincial People's Hospital Jinniu Hospital, Chengdu 610000, Sichuan, PR China; [5]Clinical Trial Center, West China Hospital, Sichuan University, Chengdu 610000, Sichuan, PR China; [6]Department of Hematology, The Affiliated Hospital of North Sichuan Medical College, Chengdu 610000, Sichuan, PR China; [7]Department of Hematology, West China Hospital, Sichuan University, Chengdu 610000, Sichuan, PR China; [8]The First Affiliated Hospital, Department of Hematology, Hengyang Medical School, University of South China, Hengyang 421200, Hunan, PR China*

Received August 3, 2022; Accepted February 17, 2023; Epub April 15, 2023; Published April 30, 2023

**Abstract:** Objective: Diffuse large B-cell lymphoma (DLBCL) is an aggressive B-cell non-Hodgkin's lymphoma. Invasive DLBCL cells are likely to metastasize into extranodal tissue (e.g., the central nervous system) that is difficult for chemotherapy drugs to penetrate, seriously affecting patient prognosis. The mechanism of DLBCL invasion remains unclear. This study investigated the association between invasiveness and platelet endothelial cell adhesion molecule-1 (CD31) in DLBCL. Methods: This study consisted of 40 newly diagnosed DLBCL patients. Differentially expressed genes and pathways in invasive DLBCL cells were identified using real-time polymerase chain reaction, western blotting, immunofluorescence, and immunohistochemical staining, RNA sequencing, and animal experiments. The effect of CD31-overexpressing DLBCL cells on the interactions between endothelial cells was determined using scanning electron microscopy. The interactions between CD8+ T cells and DLBCL cells were examined using xenograft models and single-cell RNA sequencing. Results: CD31 was upregulated in patients with multiple metastatic tumor foci compared to patients with a single tumor focus. CD31-overexpressing DLBCL cells formed more metastatic foci in mice and shortened mouse survival time. CD31 disrupted the tight junctions between endothelial cells of the blood-brain barrier by activating the osteopontin-epidermal growth factor receptor-tight junction protein 1/tight junction protein-2 axis through the protein kinase B (AKT) pathway, enabling DLBCL to enter the central nervous system to form central nervous system lymphoma. Furthermore, CD31-overexpressing DLBCL cells recruited CD31+ CD8+ T cells that failed to synthesize interferon-γ (INF-γ), tumor necrosis factor-α (TNF-α), and perforin via the activated mTOR pathway. Some target genes, such as those encoding S100 calcium-binding protein A4, macrophage-activating factor, and class I b-tubulin, may be used to treat this type of DLBCL surrounded by functionally suppressed CD31+ memory T cells. Conclusions: Our study suggests that DLBCL invasion is associated with CD31. The presence of CD31 in DLBCL lesions could represent a valuable target for treating central nervous system lymphoma and restoring CD8+ T-cell function.

**Keywords:** CD31, diffuse large B cell lymphone, invasion, OPN, mTOR

## Introduction

Diffuse large B-cell lymphoma (DLBCL) is a cancer originating in the lymphatic system [1]. Malignant tumors are characterized by the formation of metastases. DLBCL is a heterogeneous blood tumor, reflected in the large differences in the number of tumor foci and survival among patients at initial diagnosis [2]. Tumor foci in newly diagnosed DLBCL can occur either in only one lymph node or tissue or simultaneously in multiple lymph nodes or tissues throughout the body. Various scoring systems, such as Ann Arbor staging, International Prognostic Index (IPI), NCCN-IPI, and the Deauville score, take the number of tumor foci

at initial diagnosis as one of the important parameters for evaluating patient status and prognosis. The more invasive DLBCL is, the more tumor foci are present at initial diagnosis and the worse the patient's prognosis [3]. Rituximab, cyclophosphamide, doxorubicin, vincristine, and prednisolone (R-CHOP) are first-line treatment options for DLBCL, resulting in 1-year disease-free survival of over 85% for DLBCL patients. However, some patients with invasive DLBCL do not benefit from R-CHOP and have poor results in the late disease stages [4]. Invasive DLBCL cells are likely to enter the blood-brain or blood-testis barrier. Early identification of highly invasive DLBCL cell subsets can help prevent the occurrence of central nervous system lymphoma (CNSL). Because invasive DLBCL can leave the primary lesion early and evade chemotherapeutic agents, some DLBCL patients initially benefiting from R-CHOP may later relapse with CNSL. CNSL is fatal for DLBCL patients [5]. Prophylactic intrathecal injection of chemotherapy drugs has limited significance for CNSL. Currently, the backbone of CNSL treatment is high-dose methotrexate; however, it cannot be administered to patients with impaired renal function or kidney transplantation. CNSL tumor cells often accumulate in the perivascular space [6]. CNSL may not require sufficient endothelial cells to participate in angiogenesis in the early stage, but it needs endothelial cells to participate in tumor invasion and destruction of parenchyma [7]. Therefore, studying DLBCL invasion is important for identifying new treatments [8].

Platelet endothelial cell adhesion molecule-1 (CD31) is a highly glycosylated Ig-like membrane receptor expressed by leukocytes, platelets, and endothelial cells. The full-length isoform of human CD31 is a 130 kDa type I transmembrane glycoprotein comprised of six Ig-like extracellular domains, a short transmembrane segment, and a cytoplasmic tail of varying length due to alternative splicing [9]. CD31 promotes cell migration, signal transduction, and tumor angiogenesis and inhibits apoptosis [10]. Although some research suggests that CD31 is a drug delivery marker for cardiovascular and cerebrovascular diseases [11], aberrant CD31 expression is closely associated with B-cell activity [12]. Some relapsing and refractory DLBCL cells originating from CD20-negative tumor cells limit the use of rituximab and carry antigens that can bind to CD31 [13]; however, the mechanism by which CD31 helps DLBCL cells escape from the primary tumor and enter other tissues is unclear.

Complex interactions between tumor and tissue cells regulate tumor dissemination, a process that begins early at the primary tumor site until tumor cells detach themselves from the tumor mass and start migrating into the mesenteric lymph nodes or mesentery. Osteopontin (OPN) is a key determinant of the crosstalk between cancer cells and the host microenvironment [14]. Therapeutic targeting of OPN needs to consider the heterogeneous functions of the multiple OPN isoforms with regard to cancer formation and progression [15]. OPN expression is associated with non-germinal center DLBCL, a more aggressive lymphoma variant [16]. Understanding how OPN is abnormally activated is key to elucidating the differences in DLBCL invasion. Because studies on OPN and DLBCL invasion are limited, the clinical utility of OPN as a marker of DLBCL prognosis and treatment monitoring is unclear.

Mammalian target of rapamycin (mTOR) is a serine/threonine protein kinase in the phosphoinositide 3-kinase (PI3K)-related kinase family that forms the catalytic subunit of two distinct protein complexes, mTOR Complex 1 (mTORC1) and mTOR Complex 2 (mTORC2). Extensive research has established the central role of mTOR in regulating many fundamental cell processes, from protein synthesis to autophagy, and deregulated mTOR signaling is implicated in cancer progression [17]. Early rapamycin studies showed that mTOR could block T-cell activation, a key aspect of the adaptive immune response. The mTOR signaling pathway is important for malignant B-cell growth and survival [18]. Preclinical studies in DLBCL cell lines demonstrated that mTOR inhibitor-induced CNSL cell cycle arrest was synergistic with rituximab [19]. Understanding how CD31 interacts with mTOR and promotes CNSL is key to explaining the above results. In this study, we aimed to characterize the role of CD31 in DLBCL invasion. Targeting CD31 may be a valuable strategy for reducing DLBCL cell invasion and preventing tumor progression.

## Materials and methods

### *Primary cell culture and reagents*

In order to get a more accurate study of diffuse large B-cell lymphoma (DLBCL), we directly detected newly diagnosed and relapsed/refrac-

**Table 1.** Clinical information of all patients

| | | |
|---|---|---|
| Total (N, %) | | 40 |
| Gender | | |
| Male | | 24 (60%) |
| Female | | 16 (40%) |
| Age | | |
| < 60 | | 20 (50%) |
| ≥ 60 | | 20 (50%) |
| GCB/ABC | | |
| GCB | | 20 (50%) |
| ABC | | 20 (50%) |
| Ann Arbor Staging | | |
| I-II | | 7 (17.5%) |
| III-IV | | 33 (82.5%) |
| IPI Score | Point | |
| Low risk | 0 | 1 (2.5%) |
| | 1 | 2 (5%) |
| Low to medium risk | 2 | 8 (20%) |
| High to medium risk | 3 | 10 (25%) |
| High risk | 4 | 11 (27.5%) |
| | 5 | 8 (20%) |
| NCCN-IPI Score | | |
| Low risk | 0 | 0 (0%) |
| | 1 | 3 (7.5%) |
| Low to medium risk | 2 | 0 (0%) |
| | 3 | 9 (22.5%) |
| High to medium risk | 4 | 8 (20%) |
| | 5 | 11 (27.5%) |
| High risk | 6 | 7 (17.5%) |
| | 7 | 2 (5%) |
| | 8 | 0 (0%) |
| Deauville Score | | |
| 1 | | 1 (2.5%) |
| 2 | | 3 (7.5%) |
| 3 | | 8 (20%) |
| 4 | | 11 (27.5%) |
| 5 | | 17 (42.5%) |
| Affected organs | | |
| 1 | | 7 (17.5%) |
| ≥ 2, < 5 | | 21 (52.5%) |
| ≥ 5, < 10 | | 4 (10%) |
| ≥ 10, < 20 | | 8 (20%) |

GCB: germinal center B-cell-like lymphone; ABC: activated B-cell-like lymphoma; IPI Score: international prognostic index score; NCCN-IPI Score: National Comprehensive Cancer Network-International Prognostic Index score.

tory DLBCL patient's cells. The patient's DLBCL cells helped us to further accurately elucidate the mechanism of the DLBCL cells. We used positive magnetic bead sorting to obtain higher purity B cells from lymph nodes and tumor tissues. **Table 1** provides patients information. All operations were carried out carefully in accordance with the instructions. DETACHaBEAD CD19 (Dynal, Norway) was designed to release CD19+ B cells from DLBCL patients and normal donors. CD19+ B cells released according to the instructions were pure, viable, and not activated. There were no residual magnetic beads or primary antibodies bound to the surface. The obtained DLBCL primary cell suspension was cultured in RPMI 1640 medium enriched with 100 U/ml penicillin, 100 mg/ml streptomycin and 15% fetal bovine serum (FBS). To further ensure the purity of patient DLBCL cells, we subcultured the primary cells for 4 weeks and used flow cytometer (BD Biosciences, San Jose, CA, USA) and immunohistochemistry (CD20, CD30, CD3, CK, CD38, CD138, PAX-5, CD79a, Bcl-6, Bcl-2, Mum-1, CD10, C-myc, P53 and Ki-67) to determine whether they were DLBCL cells. The mouse CD19+ B cells were released using the ImunoSep Mouse CD19+ cell positive selection kit (Precision BioMedicals Co., Ltd., Tianjin, CHN). We carefully followed the instructions to release CD19+ B cells from DLBCL mice model and healthy mice. The CD19+ B cells released from the DLBCL model mice were also subcultured for 4 weeks and the non-proliferative cells would die. This helped us ensure the tumor-derived and monoclonal of the cells. Mouse CD4+ T cells were released using Dynabeads FlowComp Mouse CD4 (Invitrogen, Carlsbad, CA). Mouse CD8+ T cells were released using Dynabeads FlowComp Mouse CD8 (Invitrogen, Carlsbad, CA). All operations were performed carefully in accordance with the instructions. All cell culture plates were maintained in a humidified incubator at 37°C in a 5% CO atmosphere. Cell culture media and supplements were purchased from Hyclone (Termo Fisher Scientific, Waltham, MA, USA). Antibodies for Western blot analysis were obtained from Abcam (Cambridge, MA, USA) and secondary antibodies were purchased from Abcam (Cambridge, MA, USA). TRIzol reagent was bought from Life Technologies (USA). AVSTIN (99.29% purity) was obtained from Shanghai Selleck Chemicals Co., Ltd. (China). Antibodies for immunohistochemistry analysis were obtained from Invitrogen (Carlsbad, CA) and secondary antibodies were purchased from Invitrogen (Carlsbad, CA).

Antibodies for immunofluorescence analysis were obtained from Abcam (Cambridge, MA, USA) and secondary antibodies were purchased from Li-Cor Corp. (Lincoln, NE, USA). The inhibitors (Odanacatib, NIK SMI1, Oroxin B, Ridaforolimus and Bevacizumab) were purchased from MedChem Express (Monmouth Junction, NJ, USA) and dissolved in DMSO. The patients DLBCL cells were treated at 5-25 μM with either inhibitor or at matched concentration of DMSO (0.1%) for 24 h.

*Western-blot analysis*

Western-blot was employed to detect the protein expressions of related genes in newly diagnosed, relapsed and refractory DLBCL patients, as well as in the cells transfected with siRNA or lentivirus. Briefly, cells were washed by phosphate buffer solution (PBS), collected, and then lysed in radioimmunoprecipitation (RIPA) assay buffer (50 mM Tris-HCl, 150 mM NaCl, 0.1% SDS, 0.5% Na-deoxycholate, 1% NP40) containing proteinase inhibitor cocktail and phosphatase inhibitor cocktail (Roche Applied Science, Indianapolis, IN, USA). The lysate was centrifuged at 12000 × g at 4°C for 20 min. The protein concentration was determined using Pierce BCA Protein Assay Kit (Thermo scientifc, Waltham, MA, USA) at 562 nm. The supernatant with equal amounts of protein (50 μg protein) was fractioned using 10% SDS-PAGE and electrophoretically transferred to Hybond-enhanced chemiluminescence membrane (GE Healthcare Life Sciences, Piscataway, NJ, USA). The membrane was blocked with 5% non-fat skim milk (Blocking-Grade Blocker; Bio-Rad) in 1 × TBST (10 mM Tris-HCl, 150 mM NaCl, 0.05% Tween-20) at room temperature for 1 h and then incubated with primary antibody (Abcam, Cambridge, MA, USA) at 4°C overnight. After being washed with PBS containing 0.1% Tween 20 (PBST), the membranes were incubated with horseradish peroxidase (HRP) conjugated with anti-IgG secondary antibodies (Abcam, Cambridge, MA, USA) for 45 min and visualized by an ECL Detection Kit (Bio-Rad). All experiments were conducted at least three times.

*Quantitative real-time PCR and PCR arrays*

Cells were washed with PBS twice and lysed with buffer RL containing a 50 × dithiothreitol (DTT) solution. Total RNA was isolated and purified from cells by RNeasy Kit (Qiagen, Hilden, Germany) according to the manufacturers' instructions, and reverse-transcribed using Omniscript Reverse Transcription Kit (Qiagen, Hilden, Germany). cDNAs were analyzed by quantitative real-time PCR using primers provided by Airui Technology Corporation (Chengdu, China) and iQ SYBR Green supermix (Bio-Rad, Singapore). The specificity, efficiency, and fidelity of PCR primers for real-time quantitative PCR were validated by checking PCR products and analyzing the melting curves. The thermal cycling conditions used in the protocol were 1 min at 94°C, followed by 40 cycles at 94°C for 10 s and at 60°C for 15 s. All experiments were performed at least three times.

*Patient samples*

Forty patients, who were diagnosed as DLBCL and received treatment at the Affiliated Hospital of Guiyang Medical College, Affiliated Hospital of North Sichuan Medical College and West China Hospital of Sichuan University, were included in this study (**Table 1**). All patients were classified according to the ANN Arbor Staging. Relapsed and refractory patients were identified by PET-CT and pathological biopsy after standard therapy. The clinical information of all patients was shown in **Table 1**. We also collected samples from 40 normal donors. We obtained all samples by ultrasound-guided puncture and resection procedures. The study was approved by the institutional review board (Affiliated Hospital of the Guiyang Medical College, Affiliated Hospital of North Sichuan Medical College and West China Hospital of Sichuan University), and written informed consent was obtained in accordance with the Declaration of Helsinki before blood donation in each case. Research protocols of this study were reviewed and approved by the Ethics Committee of West China Hospital of Sichuan University and North Sichuan Medical College.

*mRNA sequencing and gene expression analysis*

Nonnecrotic tissues were carefully removed from the tumors and immediately snap-frozen at -80°C until later use for gene and protein expression analysis; the remaining tissues were fixed in formalin for histologic evaluation. Changes in the target gene expression profiles and key pathway components in the tumors

were examined through RNA sequencing analysis. For gene expression analysis, RNA was isolated from the snap frozen xenograft tumor tissue using the RNeasy Fibrous Tissue Mini Kit (Qiagen, Germantown, MA, USA) with DNAse I treatment and TRIzol Reagent (Invitrogen, Carlsbad, CA), as described in the manufacturer's protocol. The quality of RNA was assessed with Qubit2.0 Fluorometer and Agilent 2100 bioanalyzer. The sequencing libraries were prepared following the supplier's protocols for sequencing mRNA samples (Illumina, Foster City, CA, USA). The FASTQ sequence reads were aligned using the human genome hg19 TopHat (v2.0.9) application with default parameters and Bowtie (v1.0.0). The raw counts per gene in each xenograft tumor were then normalized as fragments per kilobase per million mapped reads to represent the expression level of the gene in the tumor. Differentially expressed genes were identified using the Bioconductor package DESeq2. A heatmap was generated through the color-coding of standardized log gene expression levels (mean, zero; SD, one). The RNA sequencing data were subjected to gene set enrichment analysis (GSEA; http://www.broadinstitute.org/gsea) to identify the enrichment or depletion of defined gene expression signatures in reference to the database (NR, SwissProt, PFAM, GO, KEGG and STRING). The genes that were significantly regulated between the experiment group and vehicle control were selected based on a false discovery rate (FDR) of $< 0.05$ and absolute fold change of $\geq 2$ on pretransformed expression on a log2 scale.

*Hematoxylin-eosin (HE) staining*

Fresh tissues were put into the stationary solution (10% formalin). The cell protein was denatured and solidified. The tissue was fixed for 24 h. After pruning the tissue, we put it into the embedding box and rinse it with water for 30 min. Tissue blocks were dehydrated using different concentrations of alcohol and placed in xylene. The transparent tissue blocks were placed in the dissolved paraffin wax and stored in the wax box. After the paraffin wax was completely immersed in the tissue, the paraffin was embedded. A slice machine was used to slice the block after the block was cooled and solidified. The slices were stained with hematoxylin solution for several minutes. The slices were placed in the acid and ammonia water for a few seconds respectively. After 1 hour of washing, we put it into the distilled water for a moment, dehydrating in alcohol for 10 min, and staining for 2-3 min. The stained sections were dehydrated by pure alcohol, translucented by xylene, and sealed with cover glass. All experiments were conducted at least three times.

*Scanning electron microscope*

Mice were sacrificed by cervical dislocation, and fontanelles were carefully isolated. The intact brain tissue of the mice was isolated. The vascular choroids, which were attached to the fontanelles and brain tissue, were bluntly isolated. The above parts were fixed with glutaraldehyde for 24 h, dehydrated by 40%, 60%, 80% and 100% alcohol, and kept in the oven for 5 min. The dried samples were adhered to the sample holder. The sample holder was placed in the steaming chamber. The ventilation valve was opened, and the surface of the samples were plated with a metal film so that the electron beam could penetrate the sample to form an image. The samples were observed by scanning electron microscope. All experiments were conducted at least three times.

*Virus and siRNA transfection*

Lentivirus and small interfering RNA (siRNA) targeting human were selected with Invitrogen designer software. For example, retroviruses were generated by transfecting empty plasmid vectors containing the enhanced green fluorescence protein (EGFP) or vectors containing human CD31-EGFP/siRNA-CD31-EGFP into 293FT packaging cells, using the FuGENE HD6. Lentiviral stocks were concentrated using Lenti-X concentrator, and titers were determined with Lenti-X qRT-PCR titration kit (Shanghai Innovation Biotechnology Co., Ltd., China). Finally, lentivirus-V5-D-TOPO-CD31-EGFP (L-CD31), lentivirus-V5-D-TOPO-EGFP (TOPO-EGFP), lentivirus-pRNAi-u6.2-EGFP-siCD31 (siCD31), and lentivirus-pRnai-u6.2-egfP (RNAi-EGFP) 4 recombinant lentiviral vectors were constructed. For transduction, cells were plated onto 12-well plates at the density of $2.5 \times 10^5$/well, infected with the lentiviral stocks at a multiplicity of infection of 10 in the presence of polybrene (10 μg/ml), and then analyzed by fluorescence microscopy (Olympus, Tokyo,

Japan) and Western blotting at 48 h after transduction.

*Immunohistochemistry*

The slides were placed in a mixture of potassium dichromate and $H_2SO_4$ and then washed to remove residual potassium dichromate and $H_2SO_4$ (approximately one hour). Then, the slides were soaked in alcohol, placed on a rack, and placed in a 37°C incubator. Some liquid paraffin was added to the iron mold. The tissue was placed in paraffin after paraffin cooling. Paraffin machine was used to section the embedded tissue. Sections were deparaffinized using xylene and various concentrations of alcohol. Sections were heated to expose the site of the antigen and repair the antigen. Serum was used to block non-specific sites. Primary and secondary antibodies (Abcam, Cambridge, MA, USA) were added, followed by strept avidin-biotin (SABC). Dehydrating was performed after addition of chromogen and counterstaining.

*Animals and treatments*

In the experiment, we selected two kinds of male mice (BALB/c-Nude and C57BL/6Ly5.2) for different experiments. Male C57BL/6Ly5.2 and BALB/c-Nude mice weighing 18 to 20 g were purchased from the Institute of Laboratory Animal Sciences (PUMC, Beijing, China). The mice were cultured in specific pathogen free (SPF) class animal laboratory. After adapting to the environment, the mice were divided into 16 groups randomly. Eight groups of 72 mice served as the experiment group and were injected with EXP-1 DLBCL cells. The other groups of mice were EXP-2 DLBCL cells group. Each mouse was injected with $3 \times 10^7$ DLBCL cells. All mice were injected via tail vein every day for one week. The survival time of mice were recorded and analyzed. Hematoxylin and eosin (HE) staining was used to detect DLBCL cells infiltration in thyroid, lymph nodes, spleen, ovary and mesentery. The experiment strictly followed the Helsinki declaration and passed the ethical examination of animal experiments in Sichuan University and North Sichuan Medical College (Ethical approval number: 2020ER036-1 and 2021025A).

*Immunofluorescence*

The cells or tissues were washed with PBS twice, and fixed using a cross-linking agent such as paraformaldehyde. Cells or tissues were permeabilized before adding the antibody for incubation to ensure that the antibody can reach the antigenic site. The selection of permeabilizers should fully consider the properties of antigenic proteins. The permeabilization time was generally 15 min. After permeabilization, they were washed with PBS. Cells were blocked with blocking solution for 30 min. Incubated primary antibodies for 1 h at room temperature or overnight at 4°C. Then washed with PBST. Incubated with secondary antibody for 1 h at room temperature in the dark. Washed with PBST for 3 times and rinsed with distilled water. Fluorescence microscopy was performed after adding the mounting medium.

*Flow cytometry*

The treated cells were stained according to the instructions of the Lymphocyte subsets Kit (Invitrogen, Carlsbad, CA). After being stained at room temperature for 15 min in the dark, cells were detected using the FACScan flow cytometer (Becton-Dickinson, FranKlin Lakes, NJ), and the data were analyzed using CellFIT software. The experiments were conducted according to the protocol provided by the manufacturer. All experiments were conducted at least three times.

*Single-cell RNA sequencing*

The cell suspension was loaded into Chromium microfluidic chips with 3' (v2 or v3, depends on project) chemistry and barcoded with a 10 × Chromium Controller (10 × Genomics). RNA from the barcoded cells was subsequently reverse-transcribed and sequencing libraries constructed with reagents from a Chromium Single Cell 3' v2 (v2 or v3, depending on project) reagent kit (10 × Genomics) according to the manufacturer's instructions. Sequencing was performed with Illumina (HiSeq 2000 or NovaSeq, depends on project) according to the manufacturer's instructions (Illumina). Raw reads were demultiplexed and mapped to the reference genome by UMI-tools (version 1.0.1, Smith et al., 2017) using default parameters. All downstream single-cell analyses were performed using Seurat (version 3.1.0, Satija et al., 2015) unless specifically mentioned. In brief, for each gene and each cell barcode (filtered by UMI-tools), unique molecule identifiers were counted to construct expression matrices. Secondary filtration was done by Seurat: A gene with expression in more than 3 cells was con-

sidered as expressed, and each cell was required to have at least 200 expressed genes. The red cells and dead cells were also filtered out.

*Ethics approval*

The experiment strictly followed the Helsinki declaration and passed the ethical examination of animal experiments in Sichuan University and North Sichuan Medical College (Ethical approval number: 2020ER036-1 and 2021025A).

*Statistical analysis*

All operations were carried out carefully in accordance with the instructions. Statistical analyses were performed using Prism 9 (GraphPad Software). The experiments were performed in biological triplicates each time and independently repeated at least 3 times. Data are presented as the mean ± S.E.M. Student's t-test (two-tailed) was used to compare differences between the control and experimental groups. For all statistical analyses, differences were labeled as *, $P < 0.05$; **, $P < 0.01$; ***, $P < 0.001$.

## Results

*CD31 overexpression in patients with DLBCL infiltration into multiple tissues*

To study the genes related to DLBCL metastasis, we compared gene expression in primary tumor tissue from newly diagnosed DLBCL patients and normal donor lymph node tissue (**Figure 1A**). Notably, ten patients with DLBCL invasion into multiple tissues (e.g., thyroid, mesentery, testis, and bone marrow) had significantly higher CD31 mRNA expression (**Figure 1B**). Immunohistochemistry (IHC) showed that the tissues of these ten patients were infiltrated by CD31-overexpressing DLBCL cells (**Figure 1C**). Western blotting showed that CD31, Indian blood group (CD44), and intercellular adhesion molecule 1 (ICAM-1) were also overexpressed in these patients (**Figure 1D**). CD31 mRNA expression was higher in newly diagnosed DLBCL patients with multiple tissues infiltrated by DLBCL cells (2-DLBCL) than in newly diagnosed DLBCL patients with a single tissue infiltrated by DLBCL cells (1-DLBCL) (**Figure 1E**). Western blotting also showed higher CD31 levels in 2-DLBCL than in 1-DLBCL (**Figure 1F**). Although some newly diagnosed patients had only a single tissue infiltrated at diagnosis (3-DLBCL), CD31 mRNA levels were higher when DLBCL cells invaded multiple tissues, and these patients had recurrent disease or progressed to treatment-refractory disease (4-DLBCL) (**Figure 1G**). IHC also showed CD31-positive DLBCL cells in the new metastases (**Figure 1H**). These patients with multiple metastases had higher CD44 and ICAM-1 levels (**Figure 1I**). R-CHOP had no significant effect on CD31 (**Figure 1J**).

*DLBCL invasion is positively correlated with CD31*

To further determine whether CD31 was a key factor for the invasion of DLBCL cells, we injected DLBCL cells expressing different levels of CD31 into C57BL/6Ly5.2 mice. First, we isolated patient DLBCL cells and observed their growth in culture (**Figure 2A**). Western blotting of lysates from two patient DLBCL cultures (EXP-1 and EXP-2) showed that EXP-1 cells expressed higher levels of CD31, CD44, and ICAM-1 than the EXP-2 cells (**Figure 2B**). Four weeks after tail-vein injection of the patient DLBCL cells into mice, we found that the EXP-1 cells invaded more tissues than the EXP-2 cells (**Figure 2C**). EXP-1 cells were detected in various organs, including the intestinal mesentery, testis, thyroid, lymph nodes, and spleen (**Figure 2D**). The cells invading the tissues expressed CD31 and CD20 (**Figure 2E**). Notably, EXP-1 cells invaded the central nervous system (**Figure 2F**). We also compared the survival times of mice injected with EXP-1 and EXP-2 cells and found that EXP-1 mice had a shorter survival time than EXP-2 mice (**Figure 2G**). We next used siRNA-CD31 to inhibit CD31 expression in EXP-1 cells, resulting in EXP-3 cells (**Figure 2H**). Injection of C57BL/6Ly5.2 mice with EXP-3 cells resulted in a reduced tissue invasion at 4 weeks (**Figure 2I**). The survival time of EXP-3 mice was also longer than EXP-1 mice (**Figure 2J**).

*CD31 regulates DLBCL invasion through the mTOR and AKT-OPN pathways*

To further understand how CD31 affects DLBCL invasiveness, we studied the downstream genes and pathways regulated by CD31 in three samples from DLBCL patients with multiple

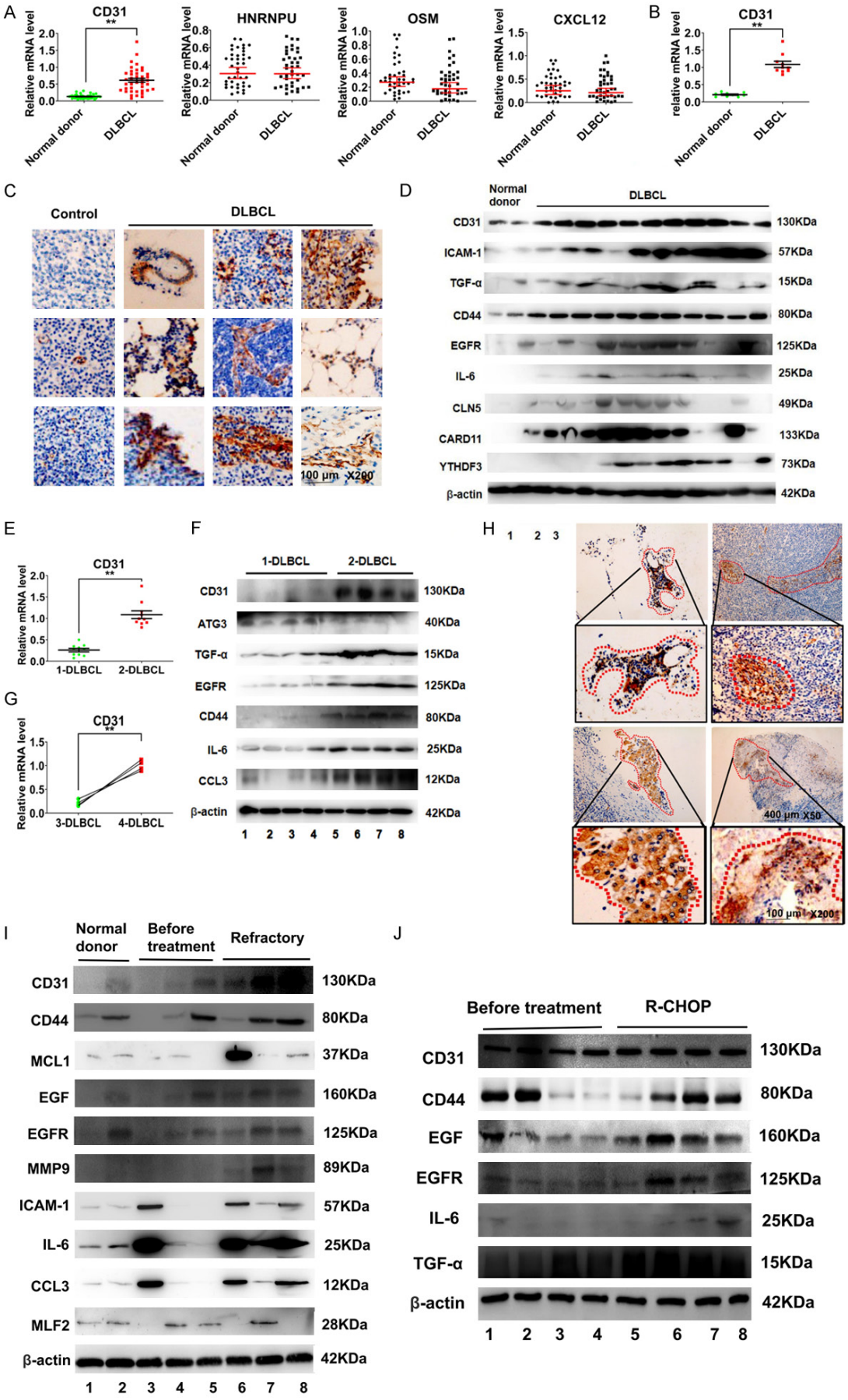
A
CD31
HNRNPU
OSM
CXCL12
Relative mRNA level
Normal donor
DLBCL
B
CD31
relative mRNA level
C
Control
DLBCL
100 μm X200
D
Normal donor
DLBCL
CD31 130KDa
ICAM-1 57KDa
TGF-α 15KDa
CD44 80KDa
EGFR 125KDa
IL-6 25KDa
CLN5 49KDa
CARD11 133KDa
YTHDF3 73KDa
β-actin 42KDa
E
CD31
1-DLBCL
2-DLBCL
F
1-DLBCL
2-DLBCL
CD31 130KDa
ATG3 40KDa
TGF-α 15KDa
EGFR 125KDa
CD44 80KDa
IL-6 25KDa
CCL3 12KDa
β-actin 42KDa
1 2 3 4 5 6 7 8
G
CD31
3-DLBCL
4-DLBCL
H
1 2 3
400 μm X50
100 μm X200
I
Normal donor
Before treatment
Refractory
CD31 130KDa
CD44 80KDa
MCL1 37KDa
EGF 160KDa
EGFR 125KDa
MMP9 89KDa
ICAM-1 57KDa
IL-6 25KDa
CCL3 12KDa
MLF2 28KDa
β-actin 42KDa
1 2 3 4 5 6 7 8
J
Before treatment
R-CHOP
CD31 130KDa
CD44 80KDa
EGF 160KDa
EGFR 125KDa
IL-6 25KDa
TGF-α 15KDa
β-actin 42KDa
1 2 3 4 5 6 7 8

**Figure 1.** DLBCL patients with multiple tissue infiltrated have significant overexpression of CD31. A. Real-time PCR was used to detect differential gene expression in 40 normal donors and 40 newly diagnosed DLBCL patients. B. Real-time PCR was used to detect the differential gene expression between DLBCL patients and normal donors. These 10 patients had multiple tissues infiltrated by DLBCL cells. C. IHC was used to detect the expression of CD31 in tissues infiltrated by DLBCL. Scale bar = 100 μm. The magnification is 200 times. D. Western-blot was used to detect differential gene expression between DLBCL patients and normal donors. These patients had multiple tissues infiltrated by DLBCL cells. E. Real-time PCR was used to detect the CD31 in 1-DLBCL patients and 2-DLBCL patients. 1-DLBCL were newly diagnosed DLBCL patients with single tissue infiltrated by DLBCL cells. 2-DLBCL were newly diagnosed DLBCL patients with multiple tissues infiltrated by DLBCL cells. F. Western-blot was used to detect the gene expression. G. Real-time PCR was used to detect the CD31 expression. 3-DLBCL were DLBCL patients with single tissue infiltrated by DLBCL cells. 4-DLBCL were relapse/refractory patients with multiple tissues infiltrated by DLBCL cells. H. IHC was used to detect CD31 in 4-DLBCL. I. Western-blot was used to detect gene expression. Scale bar = 100 μm. The magnification is 200 times. Scale bar = 40 μm. The magnification is 50 times. J. Western-blot was used to detect the effect of R-CHOP treatment regimen to CD31. **Table 1** is 40 DLBCL patients information. DLBCL: diffuse large B cell lymphoma; IHC: immunohistochemistry; Real-time PCR: real-time polymerase chain reaction. All experiments were repeated at least in triplicate ($^{*}P < 0.05$, $^{**}P < 0.01$, $^{***}P < 0.001$).

metastases and three normal donor lymph node samples using RNA sequencing (**Figure 3A**). Next, we sequenced samples from three DLBCL patients with tumor cell invasion in multiple tissues and three DLBCL patients with a single tumor focus (**Figure 3B**). Finally, we also performed RNA sequencing analysis on the differentially expressed genes in three DLBCL-invaded mouse lymph nodes and three normal mouse lymph nodes (**Figure 3C**). The analysis identified 92 differentially expressed genes in common between the three RNA sequencing datasets (**Figure 3D**). Our enrichment analysis showed that these genes were associated with mTOR pathways, adherens junctions, and the regulation of cell adhesion (**Figure 3E**). Using gene sequence enrichment analysis, we found that mTOR and OPN may be associated with CD31 (**Figure 3F**).

*CD31 promotes DLBCL metastasis by activating the AKT-OPN-epidermal growth factor receptor (EGFR) pathway*

OPN was overexpressed in tissues and organs invaded by CD31-overexpressing DLBCL cells (**Figure 4A**). Western blotting showed that siRNA-CD31 decreased CD31, phosphorylated-protein kinase B (p-AKT), OPN, C-C motif chemokine ligand 3 (CCL3), ICAM-1, and EGFR levels but upregulated E-cadherin and b-catenin in CD31-overexpressing DLBCL cells. The AKT pathway inhibitor GSK690693 reduced p-AKT, OPN, CCL3, ICAM-1, and EGFR levels and upregulated E-cadherin and β-catenin in CD31-overexpressing DLBCL cells. However, the OPN inhibitor odanacatib only inhibited OPN, CCL3, ICAM-1, and EGFR protein expression and upregulated E-cadherin and β-catenin in these cells (**Figure 4B**). Only siRNA-CD31 inhibited DLBCL cell invasiveness (**Figure 4C**). In addition, siRNA-CD31 extended the survival time of the mice (**Figure 4D**). We next overexpressed CD31 in four groups of DLBCL cells that lacked CD31 expression by lentiviral transduction (**Figure 4E**). Four weeks after the injection of these cells into mice, we observed that the infiltrated tissues were destroyed by the CD31-overexpressing DLBCL cells (**Figure 4F**). We hypothesized that these DLBCL cells might infiltrate the tissues by crossing the endothelial cells. The vascular endothelial cells of the brain were structurally intact in the control group. In contrast, the vasculature in the experimental group was thin, and the endothelial cells had a loose structure. Moreover, some DLBCL cells had broken through the vasculature and penetrated the intracranial area (**Figure 4G**). The gaps between normal endothelial cells were closed by tight junctions (TJs), limiting the movement of cells from one side to the other (**Figure 4H**). The TJs of the vessels around the tumor tissue were destroyed and opened (**Figure 4I**). Thus, the two sides of the endothelium became permeable to the DLBCL cells (**Figure 4J**). Abnormal TJs detached from the vascular membrane. Their mitochondria became swollen with sparse internal cristae (**Figure 4K**). DLBCL destroyed the TJs through the CD31-OPN-EGFR pathway by inhibiting zonula occludens (ZO)-1 and ZO-2 (**Figure 4L**).

*CD31 blocks normal T-cell function*

Odanacatib and GSK690693 did not completely inhibit the invasion of DLBCL cells into extranodal tissues. We hypothesized that this finding might be related to the immune cells. We made

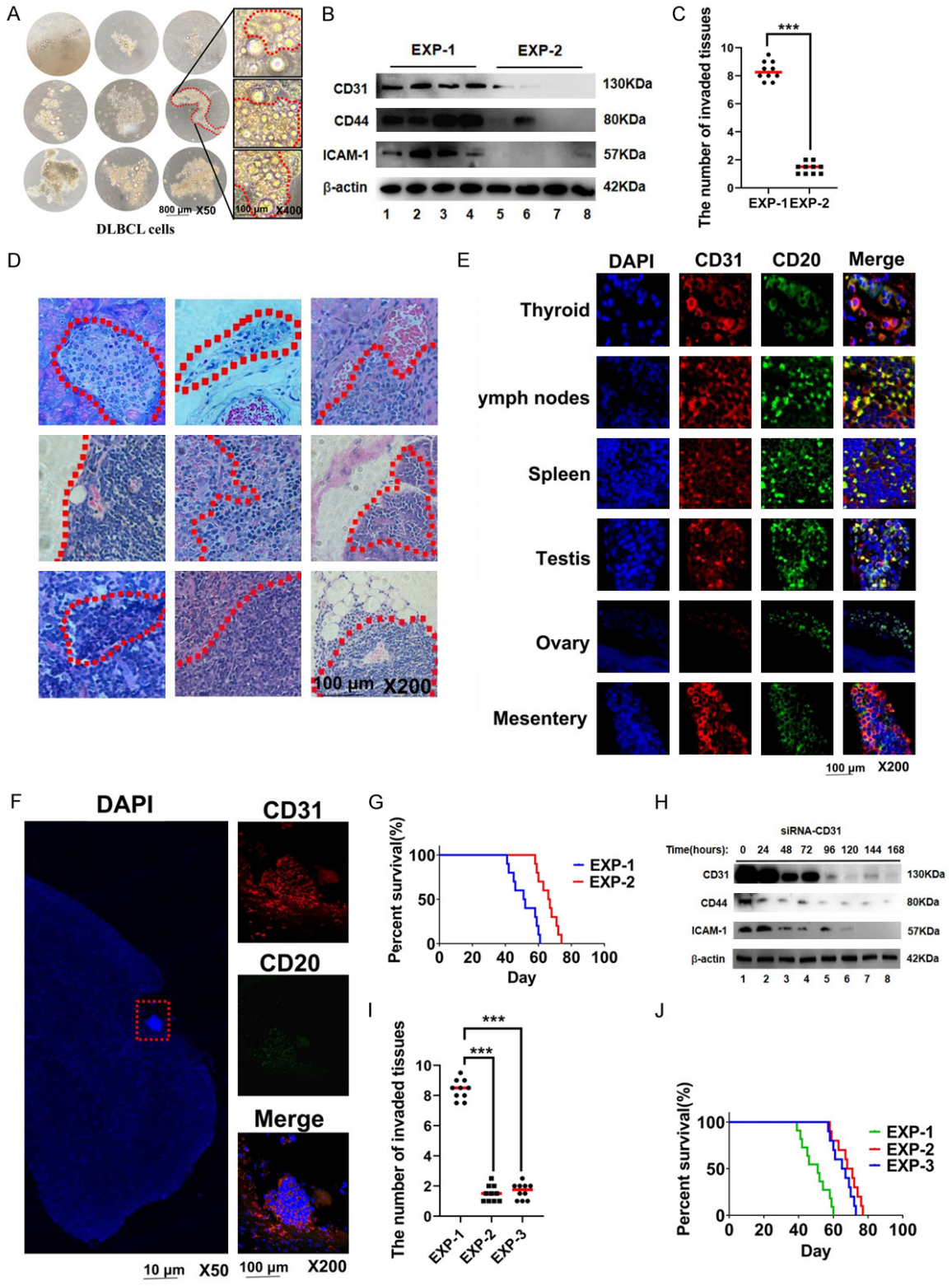


**Figure 2.** The invasion of DLBCL is positively correlated with CD31. A. We used DETACHaBEAD CD20 to release DLBCL cells from DLBCL tumour tissues. The cells were observed at different times using light microscopy. Scale bar = 800 μm. The magnification is 50 times. Scale bar = 200 μm. The magnification is 400 times. B. The gene expressions of DLBCL cells (EXP-1 cells and EXP-2 cells) were detected by Western-blot. C. 3 × $10^7$ EXP-1 cells and EXP-2 cells were injected into C57BL/6Ly5.2 mice through the tail vein. The number of invaded tissues were calculated in the fourth week. D. HE staining was used to detect tissues invaded by EXP-1 DLBCL cells. Scale bar = 100 μm. The magnification is 200 times. E. IF was used to detect the gene expression of DLBCL cells invasion tissues. Scale

bar = 100 μm. The magnification is 200 times. F. IF was used to detect EXP-1 central nervous system lymphoma (CNSL) tumour tissue. G. The survival time of EXP-1 and EXP-2 mice. Scale bar = 10 μm. The magnification is 50 times. Scale bar = 100 μm. The magnification is 200 times. H. Western-blot was used to detect the effect of siRNA-CD31 on EXP-1 cells (EXP-3) at different time. I. The number of invaded tissues in the EXP-1, EXP-2 and EXP-3 were calculated in the fourth week. J. The survival time of EXP-1, EXP-2 and EXP-3 mice. IF: Immunofluorescence. All experiments were repeated at least in triplicate ($^{*}P < 0.05$, $^{**}P < 0.01$, $^{***}P < 0.001$).

xenograft models by implanting tumor lymph nodes into the necks of C57BL/6Ly5.2 mice (**Figure 5A**). After 3 weeks, we removed the tumor lymph nodes and analyzed them by HE staining. All the tumor lymph nodes formed a layer outside composed of T cells (**Figure 5B**). However, CD31-overexpressing tumor lymph nodes had fewer T cells (**Figure 5C**). Moreover, the T cells from the CD31-overexpressing tumor lymph node group had more CD31 markers on their surfaces, and these CD31+ T cells were mostly CD8+ T cells (**Figure 5D**). We used single-cell RNA sequencing to analyze the CD8+ T cells from the CD31-overexpressing tumor lymph nodes. The mTOR pathway was activated in CD8+ T cells overexpressing CD31. We believe the CD31 was coexpressed with mTOR in the CD8+ T cells (**Figure 5E**). The expression levels of IFN-γ, perforin, and TNF-α were reduced in these mTOR-activated CD8+ memory T cells (**Figure 5F**). CD31 helped DLBCL cells inhibit the function of the CD8+ T cells through cell-to-cell contact, making this part of DLBCL cells easier to metastasize. Therefore, studying the expression of genes in DLBCL cells encoding proteins that interact with CD8+ T cells will be helpful for salvage therapy. To this end, we detected abnormally high (e.g., S100A4) or low (e.g., TUBA1B) expression of such genes in the CD31-overexpressing DLBCL cells.

## Discussion

Even when a primary lesion is controlled by first-line agents, unpredictable and untraceable metastases seriously affect patient prognosis. Searching for ideal markers of tumor invasion plays an important role in treating and identifying patients with poor prognoses. These markers could identify therapeutic targets related to metastasis, providing insights into the distribution of tumor cell subsets and gene expression differences between primary and metastatic tumors [20]. Approximately one-third of lymphomas are DLBCL, the most commonly occurring form of non-Hodgkin lymphoma in the western world [21]. In addition, accurate assessment of tumor burden is a prerequisite for improving DLBCL patient prognosis. Flourine-18 fluorodeoxyglucose positron emission tomography/computed tomography combined with the IPI score can effectively predict the prognosis of DLBCL patients after intermediate treatment [22]. Some studies have used CD31 as a marker of blood vessels, and a growing body of evidence points to the therapeutic potential of CD31 agonists in atherothrombosis [23]. Excess CD31 on the surface of leukemic cells promotes a homotypic interaction with marrow endothelial cells, resulting in higher transendothelial migration [24]. Moreover, CD31 expression in acute lymphoblastic leukemia (ALL) cells enhances the adhesion and migration of ALL cells to human brain-derived microvasculature endothelial cells [25]. The combination of multiple molecular cell surface markers (e.g., CD19, CD20, CD45, and CD3) can help identify lymphoma subtypes and targeted therapies; however, CD31 is not currently included.

A case of DLBCL with strong abnormal CD31 expression was reported in Blood in 2018, leading researchers to pay attention to its importance [26]. Although heterogeneous nuclear ribonucleoprotein U [27], oncostatin M [28] and C-X-C motif chemokine ligand 12 [29] have been reported to be essential for the invasion and metastasis of cancer, there was no difference in the expression levels of these genes between the 40 newly diagnosed DLBCL patients and the normal donors in our study. We found that CD31 expression was significantly higher in patients with multiple metastatic tumor foci than in normal donors. CD31 was also significantly higher in DLBCL patients with multiple metastatic tumor foci than in DLBCL patients with a single tumor focus. CD31-overexpressing DLBCL cells also expressed CD44, ICAM-1, and EGFR. CD44 mediates vascular barrier integrity by regulating CD31 expression [30]. Cell extravasation requires CD31-mediated ICAM-1-dependent tight adhesion and transendothelial migration [31]. CD31 can also counteract ICAM-1 inhibition by an AP-1 inhibitor [32] and promote tumor

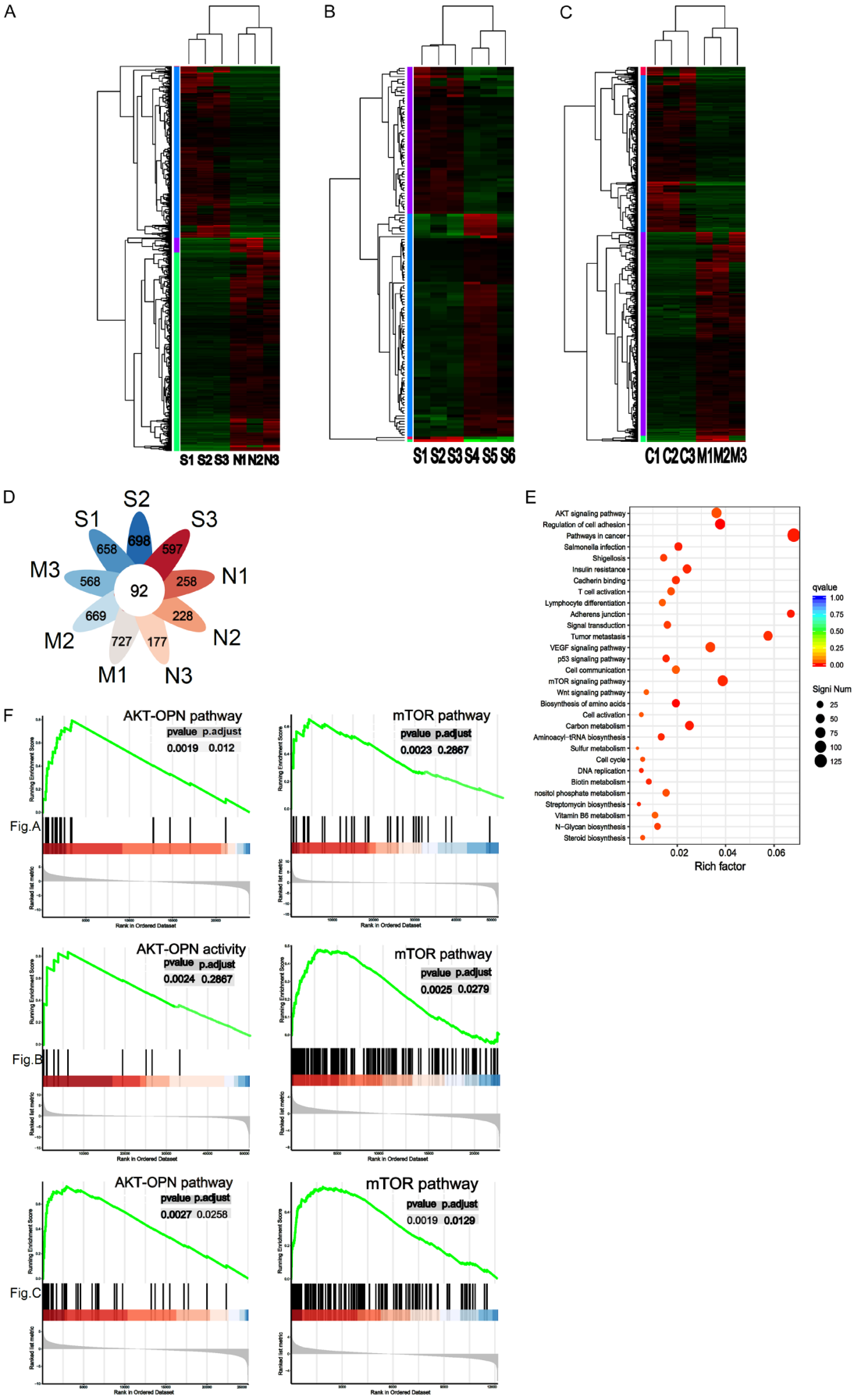
A
S1 S2 S3 N1 N2 N3
B
S1 S2 S3 S4 S5 S6
C
C1 C2 C3 M1 M2 M3
D
S1
S2
S3
M3
N1
M2
N2
M1
N3
658
698
597
568
92
258
669
228
727
177
E
AKT signaling pathway
Regulation of cell adhesion
Pathways in cancer
Salmonella infection
Shigellosis
Insulin resistance
Cadherin binding
T cell activation
Lymphocyte differentiation
Adherens junction
Signal transduction
Tumor metastasis
VEGF signaling pathway
p53 signaling pathway
Cell communication
mTOR signaling pathway
Wnt signaling pathway
Biosynthesis of amino acids
Cell activation
Carbon metabolism
Aminoacyl−tRNA biosynthesis
Sulfur metabolism
Cell cycle
DNA replication
Biotin metabolism
nositol phosphate metabolism
Streptomycin biosynthesis
Vitamin B6 metabolism
N−Glycan biosynthesis
Steroid biosynthesis
0.02
0.04
0.06
Rich factor
qvalue
1.00
0.75
0.50
0.25
0.00
Signi Num
25
50
75
100
125
F
AKT-OPN pathway
pvalue p.adjust
0.0019 0.012
mTOR pathway
pvalue p.adjust
0.0023 0.2867
Fig.A
AKT-OPN activity
pvalue p.adjust
0.0024 0.2867
mTOR pathway
pvalue p.adjust
0.0025 0.0279
Fig.B
AKT-OPN pathway
pvalue p.adjust
0.0027 0.0258
mTOR pathway
pvalue p.adjust
0.0019 0.0129
Fig.C
Running Enrichment Score
Ranked list metric
Rank in Ordered Dataset

**Figure 3.** CD31 regulates DLBCL invasion through mTOR pathway and AKT-OPN pathways. (A) RNA sequence was used to compare 3 invasive DLBCL patients' samples and 3 normal donors' lymph node samples. S1, S2 and S3 represent 3 invasive DLBCL patients' samples. N1, 2, and N3 represent 3 normal donor samples. We used heatmap to represent the results. (B) RNA sequencing was used to compare 3 DLBCL patients' samples with multiple tissue invasion and 3 DLBCL patients with single tumor foci. S4, S5 and S6 are DLBCL patients' samples with single tumor foci. (C) RNA sequencing was used to compare 3 DLBCL mice lymph nodes and 3 normal mice lymph nodes. C1, C2 and C3 represent 3 normal mice lymph nodes. (D) The common differentially expressed genes in (A-C) were analyzed. $P < 0.001$. (E) Enrichment analysis was used to analyze common differentially expressed genes. (F) GSEA (FDR < 0.05) was used to search for downstream genes and pathways regulated by CD31 in (A-C). mTOR: mammalian target of rapamycin; AKT: protein kinase B; GSEA: Gene Set Enrichment Analysis. All experiments were repeated at least in triplicate. FDR < 0.05 and absolute fold change ≥ 2. $P < 0.001$. ($^{*}P < 0.05$, $^{**}P < 0.01$, $^{***}P < 0.001$).

metastasis by focal adhesion kinase signaling pathways [33]. CD31 expression is increased in some DLBCL patients with relapsed or refractory disease. We hypothesize that R-CHOP can kill most DLBCL cells lacking CD31 expression; however, an early metastatic DLBCL subpopulation overexpressing CD31 can avoid the effects of chemotherapy and continue to proliferate, resulting in disease recurrence. When this low number of early metastatic tumor cells do not form tumor foci, it is difficult to track and treat at an early stage.

We found that DLBCL with high CD31 expression was more likely to form CNSL. CNSL occurs in approximately 5% of patients with DLBCL and is a devastating complication that often results in death within a few months [34]. Currently, methotrexate (MTX) is the backbone of CNSL treatment; however, MTX is nephrotoxic and cannot be administered to patients with impaired renal function. Moreover, immunosuppressants lead to more CNSL, which may be related to T-cell suppression and Epstein-Barr virus infection [35]. MTX cannot be used with kidney transplant patients who are chronically immunosuppressed. We think targeting CD31 may represent a new backbone for treating these patients.

CD31 affects DLBCL invasiveness by upregulating OPN through the AKT pathway. AKT is involved in the PI3K signaling pathway, which regulates the function of many downstream proteins involved in tumor cell migration. Phosphatase and tensin homolog (PTEN) is a negative regulator of PI3K-AKT signaling. PI3K-AKT dysregulation is indicated in 55% of germinal center B-cell-like (GCB) DLBCL and 14% of non-GCB DLBCL with PTEN deficiency. In addition, the PI3K-AKT signaling pathway is involved in rituximab action, and high levels of p-AKT have an adverse prognostic impact on DLBCL patients treated with R-CHOP. Conceivably, the PI3K-AKT signaling pathway has validated targets for DLBCL. Furthermore, treatment with a single agent to inhibit PI3K can trigger simultaneous activation of other related pathways, highlighting the significance of combined therapy [36]. OPN was expressed in patients with multiple tumor foci and those with relapsed or refractory disease. One study reported that MMP-7 is significantly increased in CNSL [37]. We found that DLBCL invasion was related to the simultaneous induction of matrix metallopeptidase 3 (MMP-3) and MMP-9 by OPN, and the OPN inhibitor odanacatib could inhibit MMP-3 and MMP-9. CCL3 and ICAM-1 were also inhibited by odanacatib. E-cadherin and β-catenin are both associated with cancer progression [38]. OPN simultaneously inhibited E-cadherin and β-catenin, explaining how OPN-overexpressing DLBCL cells could invade more tissues in less time and significantly shorten the survival period in mice. Therefore, we believe that odanacatib can supplement R-CHOP for treating initial highly invasive DLBCL and relapsed or refractory DLBCL with CD31 overexpression. Given that some patients with high tumor microvessel density had a worse prognosis, some clinical trials have used bevacizumab to determine whether the invasion of DLBCL is associated with CD31-induced tumor vascular growth [39]. However, bevacizumab did not show encouraging results in treating invasive DLBCL [40] because CD31 not only promotes vascular endothelial growth factor associated with the tumor-supplying microvessels but also activates OPN and downstream genes, which are not fully inhibited by bevacizumab. Therefore, relying solely on tumor microvessel density as a therapeutic guideline for using bevacizumab might delay the optimal timing of treatment for patients with invasive DLBCL.

Although OPN significantly shortened the survival time of DLBCL-bearing mice, there are many theories about how DLBCL invades tis-

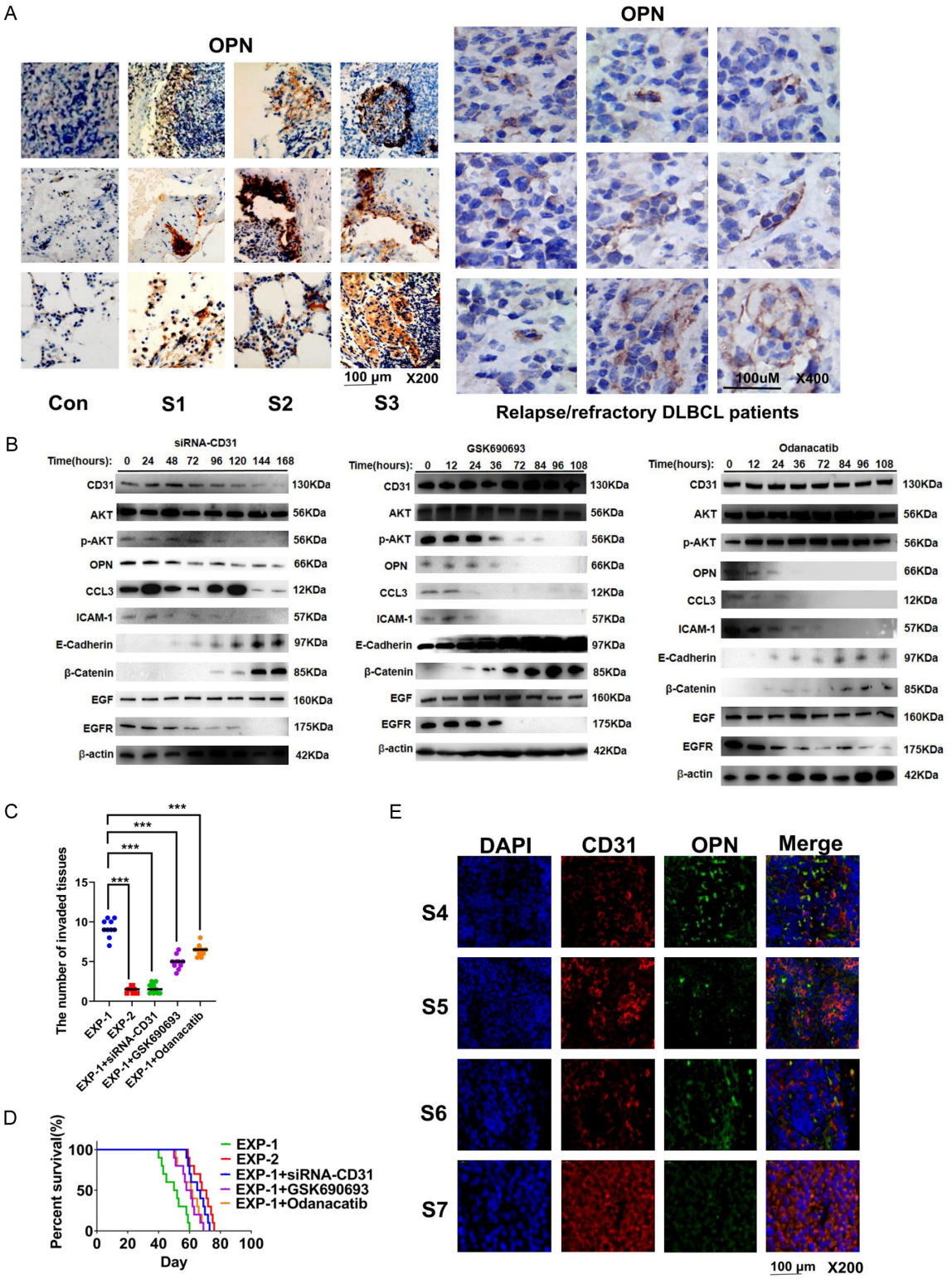
A
OPN
OPN
100 μm X200
100uM X400
Con
S1
S2
S3
Relapse/refractory DLBCL patients
B
siRNA-CD31
Time(hours): 0 24 48 72 96 120 144 168
GSK690693
Time(hours): 0 12 24 36 72 84 96 108
Odanacatib
Time(hours): 0 12 24 36 72 84 96 108
CD31 130KDa
AKT 56KDa
p-AKT 56KDa
OPN 66KDa
CCL3 12KDa
ICAM-1 57KDa
E-Cadherin 97KDa
β-Catenin 85KDa
EGF 160KDa
EGFR 175KDa
β-actin 42KDa
C
The number of invaded tissues
EXP-1
EXP-2
EXP-1+siRNA-CD31
EXP-1+GSK690693
EXP-1+Odanacatib
D
Percent survival(%)
Day
EXP-1
EXP-2
EXP-1+siRNA-CD31
EXP-1+GSK690693
EXP-1+Odanacatib
E
DAPI
CD31
OPN
Merge
S4
S5
S6
S7
100 μm X200

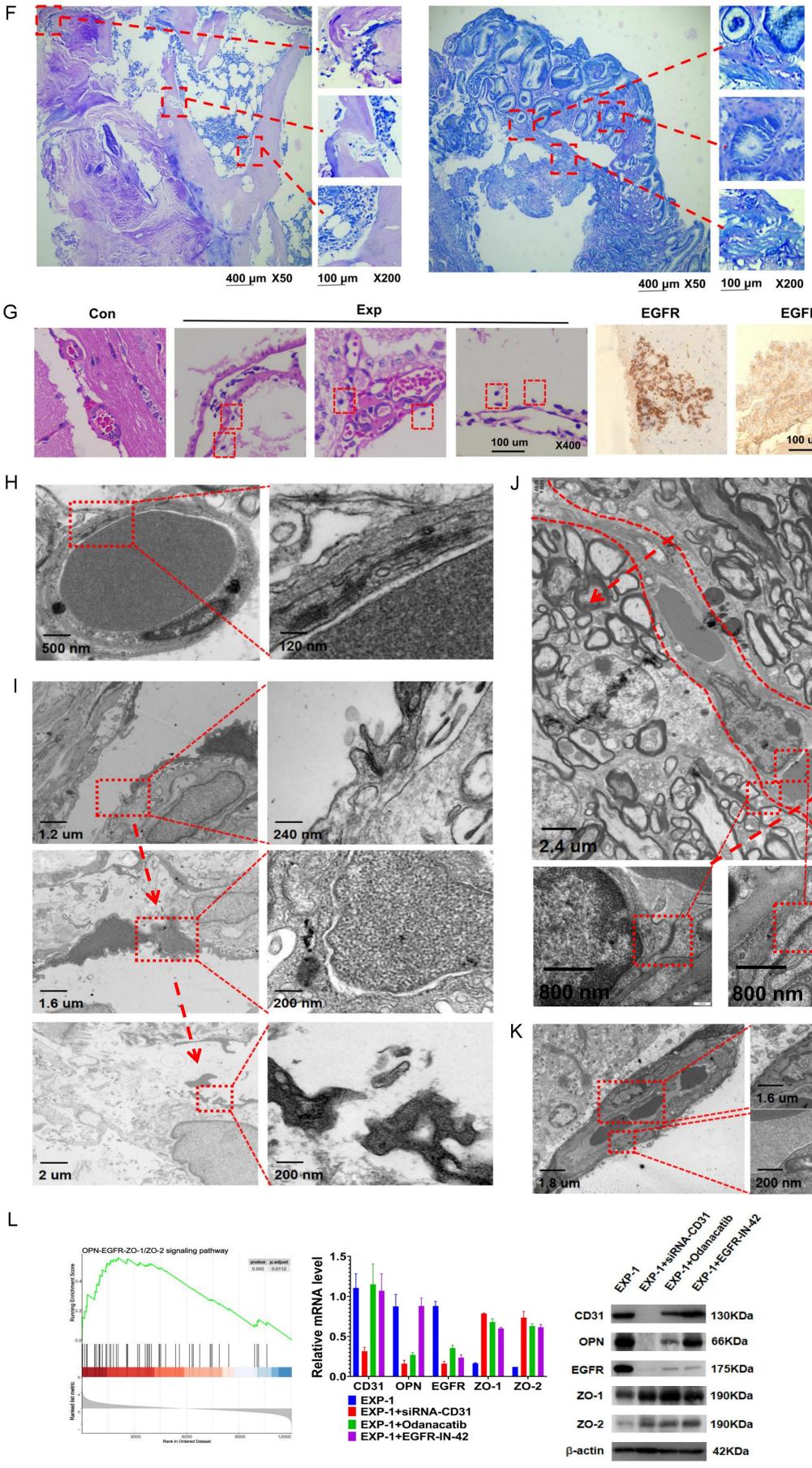
F
400 μm X50
100 μm X200
400 μm X50
100 μm X200
G
Con
Exp
EGFR
EGFR
100 um X400
100 um X400
H
500 nm
120 nm
I
1.2 um
240 nm
1.6 um
200 nm
2 um
200 nm
J
2.4 um
800 nm
800 nm
K
1.6 um
1.8 um
200 nm
L
OPN-EGFR-ZO-1/ZO-2 signaling pathway
Relative mRNA level
CD31 OPN EGFR ZO-1 ZO-2
EXP-1
EXP-1+siRNA-CD31
EXP-1+Odanacatib
EXP-1+EGFR-IN-42
EXP-1
EXP-1+siRNA-CD31
EXP-1+Odanacatib
EXP-1+EGFR-IN-42
CD31 130KDa
OPN 66KDa
EGFR 175KDa
ZO-1 190KDa
ZO-2 190KDa
β-actin 42KDa

**Figure 4.** CD31 promotes DLBCL metastasis by activating AKT-OPN-EGFR pathway. A. We used immunohistochemical staining (IHC) to detect OPN expression in tissues and organs invaded by DLBCL cells (On the left). Con represent S4, S5 and S6 DLBCL patients' samples. We also obtained samples from relapsed/refractory DLBCL patients by using needle aspiration and detected OPN by IHC (on the right). B. Western-blot was used to detect the effects of three groups (siRNA-CD31, GSK690693 and Odanacatib) on EXP-1 cells genes. DLBCL cells were treated with GSK690693 or Odanacatib (1 uM) for different hours. C. Three groups of EXP-1 cells were treated respectively with siRNA-CD31, GSK690693 or Odanacatib (1 uM) for 5 days. Then they were injected into three groups of C57BL/6Ly5.2 mice. Each group contains 10 mice. The number of invaded tissues were calculated in the 4th week. D. The survival curves of every group were analyzed. E. We detected the CD31 and OPN of 4 groups' cells by using IF. Scale bar = 100 μm. The magnification is 200 times. F. 4 group of $3 \times 10^7$ lentiviral vectors induced CD31 overexpression DLBCL cells were injected into C57BL/6Ly5.2 mice through the tail vein. The Wright' s staining was used to detected tissues infiltrated by CD31 DLBCL cells in the fourth week. Scale bar = 400 μm. The magnification is 50 times. Scale bar = 100 μm. The magnification is 200 times. G. HE staining was used to detect the structure of vessels in mice. The red circle shows DLBCL cells. Scale bar = 100 μm. The magnification is 400 times. H. TEM was used to observe the normal structure of endothelial cells. The red circles indicate the TJ that closed the spaces between endothelial cells. The magnification is shown in the figure. I. The abnormal TJ around the tumor tissue. As indicated by the arrows, the TJ went from being closed to being broken. J. DLBCL destroyed the structure of TJ. The arrow represents DLBCL cells moving to the opposite side. The red circles indicate complete TJ. K. The red circle above indicates split TJ. The red circles below indicate abnormal mitochondria. L. GSEA was used to detect EGFR-ZO-1/ZO-1 pathway. EGFR-IN-42 is an EGFR inhibitor. Real-time PCR and Western-blot were used to detect the expression ZO-1 and ZO-1. IHC: immunohistochemical staining; HE: hematoxylin-eosin staining; TEM: transmission electron microscope; TJ: tight junctions. All experiments were repeated at least in triplicate ($^{*}P < 0.05$, $^{**}P < 0.01$, $^{***}P < 0.001$).

sues. We used a CNSL model to explain a new DLBCL transfer mechanism. We found few cristae in the mitochondria of the endothelial cells, indicating the inability of these cells to maintain normal function. Furthermore, several different protein complexes form barriers between endothelial cells, including adherens junctions, gap junctions, and TJs. The CD31-AKT-OPN axis induced high EGFR expression. EGFR causes TJ instability [41]. Only after EGFR downregulation could TJs be formed via the recruitment of ZO-1 and ZO-2. These results might explain the failure of R-CHOP to prevent the metastasis of CD31-overexpressing DLBCL cells into the central nervous system.

The ability of in situ tumors to metastasize throughout the body is also related to their escape from immune surveillance [42]. Long-term survival of DLBCL in a normal immune environment is one of the causes of relapse or refractory DLBCL. Therefore, we investigated the effect of CD31 on immune cell function. As CD31 is a molecule that can bind to itself, we found that CD31-overexpressing DLBCL cells recruited CD31+ T cells. Although more CD31+ T cells were clustered around the high CD3-expressing tumor tissue, the total number of T cells was reduced. In contrast, more T cells were clustered around tumor tissues with low CD31 expression. CD31+ T cells were predominantly memory CD8+ T cells. Memory CD8+ T cells are an important component of protective immunity [43]. Although CD31+ CD8+ memory T cells clustered around the DLBCL metastases, we did not observe any anti-tumor effects. Indeed, we found significantly reduced expression of IFN-γ, TNF-α, and perforin in these CD31+ CD8+ T cells with abnormally activated mTOR. Thus, CD31 could influence memory CD8+ T-cell differentiation and activation through the mTOR pathway. The PI3K-AKT-mTOR signaling network induces programmed cell death protein 1 (PD-1) and programmed death ligand 1 (PD-L1) expression, facilitating tumor progression. Currently, combination therapy with PD-1 or PD-L1 monoclonal antibodies and small molecular inhibitors has achieved good patient outcomes. We think inhibiting mTOR can not only restore the immune recognition of T cells for tumor cells but also induce T cells to release more IFN-γ, TNF-α, and perforin. These underlying mechanisms may provide potential new targets for treating invasive DLBCL. Although inhibiting mTOR can restore some T-cell function, early targeting of invasive DLBCL cells is necessary. Our experimental data provided several novel targets for this subset of DLBCL cells surrounded by CD31+ T cells. Several limitations should be acknowledged regarding this study. The number of DLBCL patients was limited. We also did not analyze the role of CD31 in different DLBCL subtypes. Although we found some abnormally expressed genes (e.g., S100A4, MAF, and TUBB), we did not explore their potential as therapeutic targets for DLBCL.

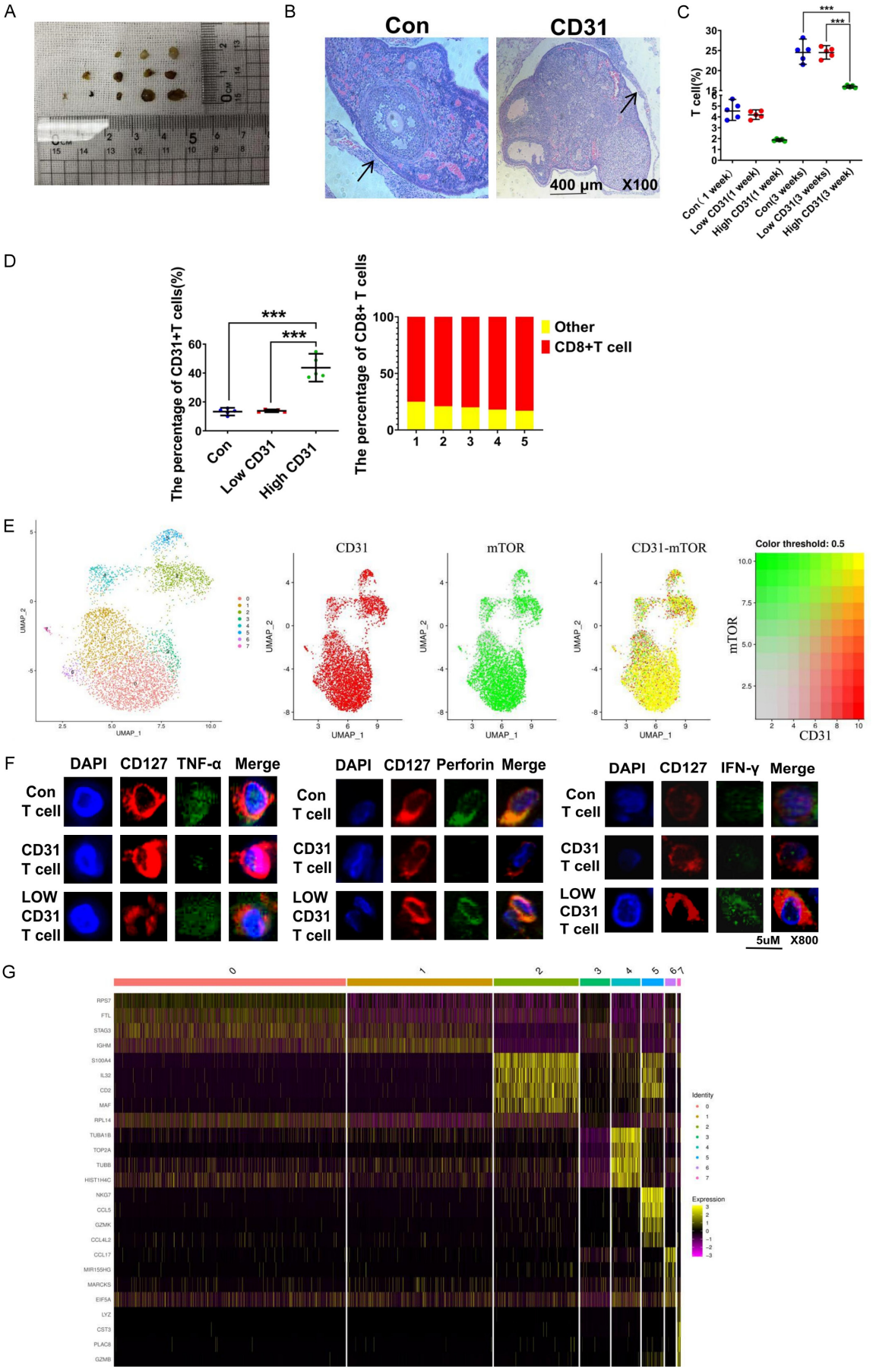
A
B
Con
CD31
400 μm X100
C
T cell(%)
Con(1 week)
Low CD31(1 week)
High CD31(1 week)
Con(3 weeks)
Low CD31(3 weeks)
High CD31(3 week)
D
The percentage of CD31+T cells(%)
Con
Low CD31
High CD31
The percentage of CD8+ T cells
Other
CD8+T cell
E
CD31
mTOR
CD31-mTOR
Color threshold: 0.5
UMAP_1
UMAP_2
F
DAPI CD127 TNF-α Merge
DAPI CD127 Perforin Merge
DAPI CD127 IFN-γ Merge
Con T cell
CD31 T cell
LOW CD31 T cell
5uM X800
G
Identity
Expression

**Figure 5.** CD31 blocks the normal function of T cells. A. In order to study the immune cells in metastasis, tumor lymph nodes of patients were directly implanted subcutaneously into the neck of C57BL/6Ly5.2 mice. B. Tumor lymph nodes were removed after 3 weeks. HE staining was used to detect lymph nodes. The arrow points to a layer of cells outside the tumor lymph nodes. Scale bar = 400 μm. The magnification is 100 times. C. Flow cytometry was used to analyze the percentage of T cells per 100,000 cells in 3 groups of tumor tissue of the same weight (0.5 g). Low CD31 represents tumor lymph nodes with Low CD31 expression DLBCL cells. High CD31 represents tumor lymph nodes with high CD31 expression DLBCL cells. D. Flow cytometry was used to analyze the type of T cells in tumor lymph nodes after 3 weeks. E. Single-Cell RNA Sequencing was used to analyse memory CD8+ T cells from the high CD31 expression tumour lymph nodes. We analyzed CD8+ T cells using UMAP and divided them into seven subgroups. F. Immunofluorescence was used to detect the TNF-α, Perforin and IFN-γ of CD8+ T cells aggregated in tumor lymph nodes. Low CD31 T cells represent T cells with Low expression of CD31. High CD31 T cells represent T cells that express high levels of CD31. Scale bar = 5 μm. The magnification is 800 times. G. RNA sequencing was used to analyze DLBCL cells. All experiments were repeated at least in triplicate ($^{*}P < 0.05$, $^{**}P < 0.01$, $^{***}P < 0.001$).

In conclusion, our study provides new insights into DLBCL cell invasion. CD31 can be used as a marker for the early detection of invasive DLBCL. Targeting CD31 may be a valuable strategy for reducing DLBCL cell invasion and preventing tumor metastasis, reducing the risk of relapse or progression to treatment-refractory disease. Current clinical agents cannot fully target these CD31-overexpressing DLBCL cells, making the selection of treatment options more difficult which worsens patient prognosis.

## Acknowledgements

We want to thank Yu Wu and Ting Niu for their discussion and technical help. We acknowledge members of Yuhuan Zheng's laboratory for the technical help and discussion. We also thank Shaoxian Shen for post correction work. The manuscript was supported by Sichuan University West China Hospital Clinical New Technology Fund Project (Grant No. 2019-088).

## Disclosure of conflict of interest

None.

**Address correspondence to:** Dr. Yongqian Jia, Department of Hematology, West China School of Medicine, West China Hospital of Sichuan University, Sichuan Provincial Laboratory of Hematopoietic Stem Cell Transplantation Centre, Chengdu 610000, Sichuan, PR China. Tel: +86-18980601198; E-mail: jia_yq@scu.edu.cn

## References

[1] Roschewski M, Staudt LM and Wilson WH. Diffuse large B-cell lymphoma-treatment approaches in the molecular era. Nat Rev Clin Oncol 2014; 11: 12-23.

[2] Li SY, Young KH and Medeiros LJ. Diffuse large B-cell lymphoma. Pathology 2018; 50: 74-87.

[3] Ruppert AS, Dixon JG, Salles G, Wall A, Cunningham D, Poeschel V, Haioun C, Tilly H, Ghesquieres H, Ziepert M, Flament J, Flowers C, Shi Q and Schmitz N. International prognostic indices in diffuse large B-cell lymphoma: a comparison of IPI, R-IPI, and NCCN-IPI. Blood 2020; 135: 2041-2048.

[4] Horvat M, Zadnik V, Setina TJ, Boltezar L, Golicnik JP, Novakovic S and Novakovic BJ. Diffuse large B-cell lymphoma: 10 years' real-world clinical experience with rituximab plus cyclophosphamide, doxorubicin, vincristine and prednisolone. Oncol Lett 2018; 15: 3602-3609.

[5] Fortin Ensign SP, Gathers D, Wiedmeier JE and Mrugala MM. Central nervous system lymphoma: novel therapies. Curr Treat Options Oncol 2022; 23: 117-136.

[6] Younes A, Sehn LH, Johnson P, Zinzani PL, Hong X, Zhu J, Patti C, Belada D, Samoilova O, Suh C, Leppa S, Rai S, Turgut M, Jurczak W, Cheung MC, Gurion R, Yeh SP, Lopez-Hernandez A, Duhrsen U, Thieblemont C, Chiattone CS, Balasubramanian S, Carey J, Liu G, Shreeve SM, Sun S, Zhuang SH, Vermeulen J, Staudt LM and Wilson W; PHOENIX investigators. Randomized phase III trial of ibrutinib and rituximab plus cyclophosphamide, doxorubicin, vincristine, and prednisone in non-germinal center B-cell diffuse large B-cell lymphoma. J Clin Oncol 2019; 37: 1285-1295.

[7] Sugita Y, Takase Y, Mori D, Tokunaga O, Nakashima A and Shigemori M. Endoglin (CD 105) is expressed on endothelial cells in the primary central nervous system lymphomas and correlates with survival. J Neurooncol 2007; 82: 249-256.

[8] Dubois S and Jardin F. Novel molecular classifications of DLBCL. Nat Rev Clin Oncol 2018; 15: 474-476.

[9] Kirschbaum NE, Gumina RJ and Newman PJ. Organization of the gene for human platelet endothelial-cell adhesion molecule-1 shows

alternatively spliced isoforms and a functionally complex cytoplasmic domain. Blood 1994; 84: 4028-4037.
[10] Feng YM, Chen XH and Zhang X. Roles of PECAM-1 in cell function and disease progression. Eur Rev Med Pharmacol Sci 2016; 20: 4082-4088.
[11] El-Galaly TC, Cheah CY, Bendtsen MD, Nowakowski GS, Kansara R, Savage KJ, Connors JM, Sehn LH, Goldschmidt N, Shaulov A, Farooq U, Link BK, Ferreri AJM, Calimeri T, Cecchetti C, Dann EJ, Thompson CA, Inbar T, Maurer MJ, Gade IL, Juul MB, Hansen JW, Holmberg S, Larsen TS, Cordua S, Mikhaeel NG, Hutchings M, Seymour JF, Clausen MR, Smith D, Opat S, Gilbertson M, Thanarajasingam G and Villa D. Treatment strategies, outcomes and prognostic factors in 291 patients with secondary CNS involvement by diffuse large B-cell lymphoma. Eur J Cancer 2018; 93: 57-68.
[12] Wilkinson R, Lyons AB, Roberts D, Wong MX, Bartley PA and Jackson DE. Platelet endothelial cell adhesion molecule-1 (PECAM-1/CD31) acts as a regulator of B-cell development, B-cell antigen receptor (BCR)-mediated activation, and autoimmune disease. Blood 2002; 100: 184-193.
[13] Vockova P, Svaton M, Karolova J, Pokorna E, Vokurka M and Klener P. Anti-CD38 therapy with daratumumab for relapsed/refractory CD20-negative diffuse large B-cell lymphoma. Folia Biol (Praha) 2020; 66: 17-23.
[14] Rangaswami H and Kundu GC. Osteopontin stimulates melanoma growth and lung metastasis through NIK/MEKK1-dependent MMP-9 activation pathways. Oncol Rep 2007; 18: 909-915.
[15] Castello LM, Raineri D, Salmi L, Clemente N, Vaschetto R, Quaglia M, Garzaro M, Gentilli S, Navalesi P, Cantaluppi V, Dianzani U, Aspesi A and Chiocchetti A. Osteopontin at the crossroads of inflammation and tumor progression. Mediators Inflamm 2017; 2017: 4049098.
[16] Barranco G, Fernandez E, Rivas S, Quezada R, Nava D, Aguilar J, Garcia A, Astudillo H, Lome C and Ruiz E. Osteopontin expression and its relationship with prognostic factors in diffuse large B-cell lymphoma. Hematol Rep 2019; 11: 7964.
[17] Saxton RA and Sabatini DM. mTOR signaling in growth, metabolism, and disease. Cell 2017; 168: 960-976.
[18] Zhang XW and Liu YB. Targeting the PI3K/AKT/mTOR signaling pathway in primary central nervous system lymphoma: current status and future prospects. CNS Neurol Disord Drug Targets 2020; 19: 165-173.
[19] Merli M, Ferrario A, Maffioli M, Arcaini L and Passamonti F. Everolimus in diffuse large B-cell lymphomas. Future Oncol 2015; 11: 373-383.
[20] Han YY, Wang D, Peng LS, Huang TY, He XY, Wang JP and Ou CL. Single-cell sequencing: a promising approach for uncovering the mechanisms of tumor metastasis. J Hematol Oncol 2022; 15: 59.
[21] Flowers CR, Sinha R and Vose JM. Improving outcomes for patients with diffuse large B-cell lymphoma. CA Cancer J Clin 2010; 60: 393-408.
[22] Jiang MQ, Chen P, Ruan XZ, Ye XW, Pan YN, Zhang J, Huang QL, Zhou WL, Wu HB and Wang QS. Interim $^{18}$F-FDG PET/CT improves the prognostic value of S-IPI, R-IPI and NCCN-IPI in patients with diffuse large B-cell lymphoma. Oncol Lett 2017; 14: 6715-6723.
[23] Caligiuri G. CD31 as a therapeutic target in atherosclerosis. Circ Res 2020; 126: 1178-1189.
[24] Gallay N, Anani L, Lopez A, Colombat P, Binet C, Domenech J, Weksler BB, Malavasi F and Herault O. The role of platelet/endothelial cell adhesion molecule-1 (CD31) and CD38 antigens in marrow microenvironmental retention of acute myelogenous leukemia cells. Cancer Res 2007; 67: 8624-8632.
[25] Akers SM, O'Leary HA, Minnear FL, Craig MD, Vos JA, Coad JE and Gibson LF. VE-cadherin and PECAM-1 enhance ALL migration across brain microvascular endothelial cell monolayers. Exp Hematol 2010; 38: 733-743.
[26] Hu SM and Wang YH. Diffuse large B-cell lymphoma with strong aberrant expression of CD31. Blood 2018; 131: 2090.
[27] Jiao WJ, Chen YJ, Song HJ, Li D, Mei H, Yang F, Fang E, Wang XJ, Huang K, Zheng L and Tong Q. HPSE enhancer RNA promotes cancer progression through driving chromatin looping and regulating hnRNPU/p300/EGR1/HPSE axis. Oncogene 2018; 37: 2728-2745.
[28] Lee BY, Hogg EKJ, Below CR, Kononov A, Blanco-Gomez A, Heider F, Xu J, Hutton C, Zhang X, Scheidt T, Beattie K, Lamarca A, McNamara M, Valle JW and Jorgensen C. Heterocellular OSM-OSMR signalling reprograms fibroblasts to promote pancreatic cancer growth and metastasis. Nat Commun 2021; 12: 7336.
[29] Yang F, Takagaki Y, Yoshitomi Y, Ikeda T, Li JP, Kitada M, Kumagai A, Kawakita E, Shi S, Kanasaki K and Koya D. Inhibition of dipeptidyl peptidase-4 accelerates epithelial-mesenchymal transition and breast cancer metastasis via the CXCL12/CXCR4/mTOR axis. Cancer Res 2019; 79: 735-746.
[30] Tsuneki M and Madri JA. CD44 regulation of endothelial cell proliferation and apoptosis via modulation of CD31 and VE-cadherin expression. J Biol Chem 2014; 289: 5357-5370.

[31] Liu Q, Yu S, Zhao W, Qin S, Chu Q and Wu K. EGFR-TKIs resistance via EGFR-independent signaling pathways. Mol Cancer 2018; 17: 53.
[32] Sawa Y, Sugimoto Y, Ueki T, Ishikawa H, Sato A, Nagato T and Yoshida S. Effects of TNF-alpha on leukocyte adhesion molecule expressions in cultured human lymphatic endothelium. J Histochem Cytochem 2007; 55: 721-733.
[33] Zhang XD, Baladandayuthapani V, Lin H, Mulligan G, Li B, Esseltine DW, Qi L, Xu J, Hunziker W, Barlogie B, Usmani SZ, Zhang Q, Crowley J, Hoering A, Shah JJ, Weber DM, Manasanch EE, Thomas SK, Li BZ, Wang HH, Zhang J, Kuiatse I, Tang JL, Wang H, He J, Yang J, Milan E, Cenci S, Ma WC, Wang ZQ, Davis RE, Yang L and Orlowski RZ. Tight junction protein 1 modulates proteasome capacity and proteasome inhibitor sensitivity in multiple myeloma via EGFR/JAK1/STAT3 signaling. Cancer Cell 2016; 29: 639-652.
[34] Clevers H and Nusse R. Wnt/β-catenin signaling and disease. Cell 2012; 149: 1192-1205.
[35] Koubska E, Weichet J and Malikova H. Central nervous system lymphoma: a morphological MRI study. Neuro Endocrinol Lett 2016; 37: 318-324.
[36] Wang L and Li LR. R-CHOP resistance in diffuse large B-cell lymphoma: biological and molecular mechanisms. Chin Med J (Engl) 2021; 134: 253-260.
[37] Matsumoto T, Kumagai J, Hasegawa M, Tamaki M, Aoyagi M, Ohno K, Mizusawa H, Kitagawa M, Eishi Y and Koike M. Significant increase in the expression of matrix metalloproteinase 7 in primary CNS lymphoma. Neuropathology 2008; 28: 277-285.
[38] Mendonsa AM, Na TY and Gumbiner BM. E-cadherin in contact inhibition and cancer. Oncogene 2018; 37: 4769-4780.
[39] Ahmed H, James A and Enghelberg M. Successful use of intravitreal bevacizumab and methotrexate in a case of neovascularization of the iris and pseudohypopyon secondary to recurrent diffuse large B-cell lymphoma. Cureus 2022; 14: e22578.
[40] Cardesa-Salzmann TM, Colomo L, Gutierrez G, Chan WC, Weisenburger D, Climent F, Gonzalez-Barca E, Mercadal S, Arenillas L, Serrano S, Tubbs R, Delabie J, Gascoyne RD, Connors JM, Mate JL, Rimsza L, Braziel R, Rosenwald A, Lenz G, Wright G, Jaffe ES, Staudt L, Jares P, Lopez-Guillermo A and Campo E. High microvessel density determines a poor outcome in patients with diffuse large B-cell lymphoma treated with rituximab plus chemotherapy. Haematologica 2011; 96: 996-1001.
[41] Rubsam M, Mertz AF, Kubo A, Marg S, Jungst C, Goranci-Buzhala G, Schauss AC, Horsley V, Dufresne ER, Moser M, Ziegler W, Amagai M, Wickstrom SA and Niessen CM. E-cadherin integrates mechanotransduction and EGFR signaling to control junctional tissue polarization and tight junction positioning. Nat Commun 2017; 8: 1250.
[42] Kline J, Godfrey J and Ansell SM. The immune landscape and response to immune checkpoint blockade therapy in lymphoma. Blood 2020; 135: 523-533.
[43] Pollizzi KN and Powell JD. Regulation of T cells by mTOR: the known knowns and the known unknowns. Trends Immunol 2015; 36: 13-20.